SF2A 2014
J. Ballet, F. Bournaud, F. Martins, R. Monier and C. Reylé (eds)

UNDERSTANDING THE STATE OF THE GAS SURROUNDING ANDROMEDA'S BLACK HOLE.

A.-L. Melchior[1, 2] and F. Combes[1, 3]

Abstract. A millimeter CO survey has been performed at IRAM of the gas surrounding Andromeda's black hole. Several velocity components are detected supporting the presence of a relic 0.7-kpc ring, signing a possible frontal collision with M32. A multiwavelength analysis of this central field of M31 has been carried out in order to get clues on the location and state of this gas. Viaene et al. (2014) estimate in this central zone a star formation rate of order 3×10^{-4} $M_\odot\,yr^{-1}$, based on infrared data. Beside a 200 Myr A-star cluster detected close to the black hole, no trace of recent star formation is observed in UV. In parallel, Halpha gas is present but due to shocks as the [NII]/Halpha ratio is larger than 3. The issue is thus to understand why the cold molecular gas is quenched and not forming stars.

Keywords: Galaxies: kinematics and dynamics, Galaxies: ISM, Galaxies: interactions, Radio lines: galaxies

1 Introduction

M31 is usually described as a quiescent galaxy with little star formation $0.25^{+0.06}_{-0.04}\,M_\odot\,yr^{-1}$ (e.g. Barmby et al. 2006; Tabatabaei & Berkhuijsen 2010; Azimlu et al. 2011; Ford et al. 2013) and with an ultra-weak nuclear activity (del Burgo et al. 2000). While the centre of M31 hosts a massive black hole with a mass of $0.7 - 1.4 \times 10^8 M_\odot$ (Bacon et al. 2001; Bender et al. 2005), it is one of the most underluminous supermassive black hole (Garcia et al. 2010), although since 2008, it started to murmur (Li et al. 2011). The gas content of this region is small compared to the Central Molecular Zone in the Milky Way. Kruijssen et al. (2014) discuss that in the CMZ the star formation rate is 10 times weaker than in the Galactic disc. We discuss that even though our neighbouring galaxy M31 has exhausted most of its gas in the central region, the gas present there does not behave like in the main disc and does not exhibit obvious signs of star formation either.

2 CO mapping and kinematics

We map at IRAM-30m the main parts of M31's inner ring in ^{12}CO(2-1). We also observed the inner parts as described in Melchior & Combes (2013). More recently some ^{12}CO(1-0) observations with Pic-de-Bure interferometer have been performed. The kinematics thus achieved is displayed in Fig. 1. As first discussed in Melchior & Combes (2011), we observe components on both sides of the systemic velocity (-300 $\mathrm{km\,s^{-1}}$) along the minor axis. These components are decoupled from the main disc (whose expected velocity is close to systemic at these positions). Also the inner ring velocities do not rotate around the optical centre where is located the central black hole. Last, in the North-West side a weak component is detected at the systemic velocity. Due to the high inclination (77 deg) of the main large-scale disc, it could be the projection of the disc, even though it could also be a more face-on inner disc (a third component).

In Fig. 1, we also display the contours (4, 7.5 and 10 mJy/pixel) of the Herschel/PACS 100 μm map (Viaene et al. 2014). The CO is not detected in all the positions of the inner ring. The detections are weak (at the mK level) and it is probable that more gas exists below the detection threshold.

[1] LERMA, UMR8112, Observatoire de Paris, 61, avenue de l'Observatoire, Paris, F-75014, France
[2] Sorbonne Universités, UPMC Univ Paris 06, UMR8112, LERMA, F75005, Paris, France
[3] Collège de France, avenue Marcelin Berthelot, Paris, F-75005, France

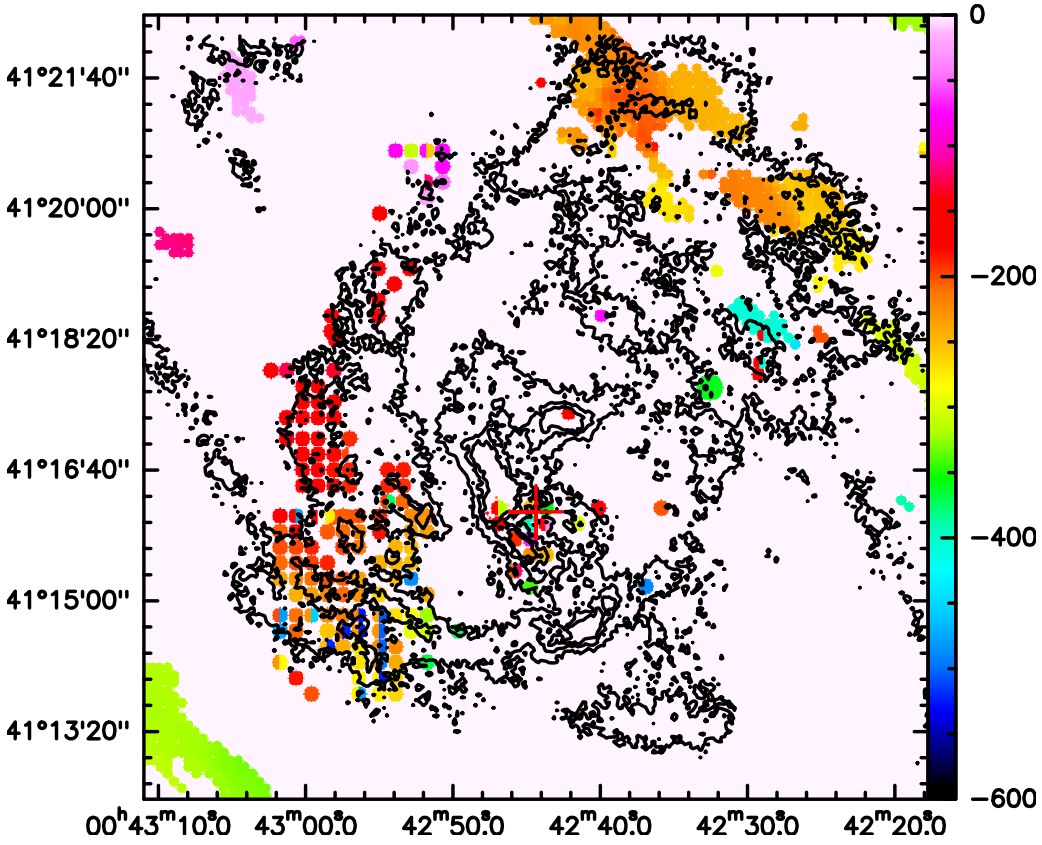

Fig. 1. CO velocities gathered from new IRAM (30m radiotelescope and Pic-de-Bure interferometer) observations and from Nieten et al. (2006) (courtesy M. Guélin). The contours (4, 7.5 and 10 mJy/pixel) correspond to the 100 μm map produced by Viaene et al. (2014). CO gas is detected along the inner ring. The velocity field exhibits several components with different position angles from the main disc rotation. Several counter-rotations are observed especially along the minor axis. The location of the optical peak (and position of the black hole) indicated with a cross is clearly off-centred.

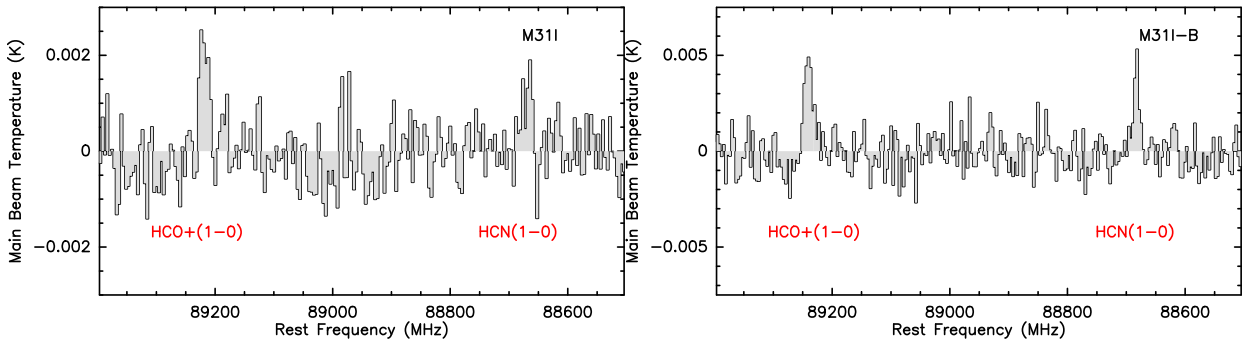

Fig. 2. Observations of dense gas in the North-West side in the inner ring. **Left:** HCO+(1-0) and HCN(1-0) lines observed at $00^h42^m29.1^s$, $+41°18'3.6"$ (J2000.0) in the rest-frame of the Andromeda galaxy. **Right:** HCO+(1-0) and HCN(1-0) lines observed at $00^h42^m26.4^s$, $+41°17'58.0"$ (J2000.0) in the rest-frame of the Andromeda galaxy.

3 Dense molecular gas

We observed at IRAM-30m with the EMIR receiver dense gas molecular lines in two bands: 87.4-91.4 GHz and 218.65-222.65 GHz. In two positions (as displayed in Fig. 2), we have detected HCO+(1-0) and HCN(1-0) corresponding to the receding component. ^{13}CO emission has been detected in 10 positions on both sides of the inner axis, with velocities corresponding to ^{12}CO. We have a detection of C^{18}O at the systemic velocity, which

Table 1. Summary of the main detections of dense gas. For each line, we provide the central velocity V_0, the FWHM velocity dispersion Δv, the main-beam temperature T_{peak} and the integrated line I_{CO}. We provide the N_{H_2} column densities computed using a standard $X_{CO} = 2 \times 10^{20}\,cm^{-2}\,(K\,km\,s^{-1})^{-1}$ following Dame et al. (2001) and assuming CO(2-1)/(1-0) ratio of 0.8 as computed in Melchior & Combes (2011) for a detection within 10" of our position M31I. The velocities V_0 and dispersions Δv flagged with a "*" have been fixed to the ^{12}CO values for the fit performed to compute I_{CO} and T_{peak}.

Parameters	M31I(2)	M31I(3)	M31I-B(1)				
	^{12}CO(2-1)				^{13}CO(2-1)		
V_0 (km/s)	-402±3	-291±9	-463±1	V_0 (km/s)	-402∗	-291∗	-463∗
Δv (km/s)	62±12	69±18	36±2	Δv (km/s)	62∗	69∗	36∗
T_{peak} (mK)	146	77	138	T_{peak} (mK)	4.6	4.9	4.5
I_{CO} (K km s^{-1})	9.6±0.5	6±1	5.3±0.2	I_{CO} (K km s^{-1})	0.30±0.06	0.36±0.06	0.48±0.04
N_{H_2} (10^{20} cm^{-2})	19±1	12±2	10.6±0.4				
	C^{18}O(2-1)				^{12}CO(1-0)		
V_0 (km/s)		-291∗		V_0 (km/s)	-412±1	-279±3	
Δv (km/s)		69∗		Δv (km/s)	34±3	46±5	
T_{peak} (mK)		4.5		T_{peak} (mK)	127	51	
I_{CO}	<0.21	0.29±0.07	<0.17	I_{CO}	4.6±0.8	2.5±0.3	
	HCO+(1-0)				HCN(1-0)		
V_0 (km/s)	-400±5		-473±4	V_0 (km/s)	-409±4		-471±2
Δv (km/s)	60±10		65±10	Δv (km/s)	25±7		32±8
T_{peak} (mK)	3.6		5.3	T_{peak} (mK)	3.0		6.1
I_{HCO+}	0.23±0.04		0.36±0.04	I_{HCN}	0.08±0.02		0.21±0.04

Table 2. Indicative abundances. For each transition, we provide the measured abundances assuming LTE and optically thin conditions. We consider the average of the measurements available for each transition. We provide in the third column the relative abundance of ^{12}CO with respect to the transition In the fourth column, we provide expected for the Galactic interstellar medium (at 4 kpc derived from Bergin et al. (1995) and Wilson & Rood (1994)). The last column provides the ratios of the transition intensities of each CO transition wih respect to ^{12}CO(2-1) and the other molecules with respect to ^{12}CO(1-0). Each set of lines has been observed with similar beams.

	Measured values (LTE)		Galactic values	
Transition	$X^{Observed}$	^{13}CO/Mol	X^{GISM}	^{12}CO/Mol
^{12}CO(2-1)	9.5×10^{-6}	1	2.8×10^{-5}	1
^{13}CO(2-1)	3.2×10^{-7}	29.7	5.28×10^{-7}	53
C^{18}O(2-1)	2.9×10^{-7}	32.3	8.56×10^{-8}	327
Transition	$X^{Observed}$	^{12}CO(1-0)/Mol	X^{GISM}	^{12}CO(1-0)/Mol
^{12}CO(1-0)	1.65×10^{-5}	1	2.8×10^{-5}	1
HCN(1-0)	1.29×10^{-10}	1.29×10^{5}	1.9×10^{-9}	1.57×10^{5}
HCO+(1-0)	2.10×10^{-10}	0.79×10^{5}	4.7×10^{-10}	1.35×10^{5}

does not correspond to the HCN and HCO+ detection. The characteristics of the components with more that 3 lines are presented in Tab. 1. Beside the ^{12}CO(2-1) and (1-0) measurements, all the detections are weak with main-beam temperatures at the mK level. We measure $I_{HCN}/I_{CO} = 1/58$. This is quite different from values observed for starbursts in the range 1/3-1/10. It is quite typical of Galactic values. If one assumes that the gas is in Local Thermal Equilibrium and optically thin, one can compute the abundances of the gas in each detected component and transition. Viaene et al. (2014) has computed a dust temperature of 20 K at the corresponding positions. We thus assume a kinetic temperature of 20 K. The results are provided in Tab. 2, together with abundances measured in the Milky Way. The measured ^{12}CO /C^{18}O ratio is a factor 10 times weaker than expected. As C^{18}O is optically thin, this ratio is due to the fact that ^{12}CO is optically thick. However, the C^{18}O intensity is comparable with the measured ^{13}CO intensity. Rather than a relative excess of C^{18}O, one could rather argue for a deficit of ^{13}CO, since such a ^{13}CO deficit was first observed by Casoli et al. (1991) in mergers. The ^{13}CO is under-abundant with respect to C^{18}O. Davis (2014) also find an anticorrelation of ^{13}CO and the star formation and gas surface densities in local galaxies. This could be the signature of a 200 Myr old

starburst triggered by the collision with M32 proposed by Block et al. (2006).

4 Conclusions

We have mapped in CO the inner ring of M31. The kinematics display a complex configuration along the minor axis with multiple components along the line of sight (identified by different velocities). In the North-West side of the inner ring, several dense gas lines have been detected. A simple analysis assuming that the gas is in Local Thermal Equilibrium and optically thin (except for ^{12}CO) shows that the abundances do not correspond to the Galactic values. We argue that the observed deficit of ^{13}CO with respect to C^{18}O and excess of HCN(1-0) with respect to HCO+(1-0) could be due to a 200 Myr old starburst which could have been triggered by a frontal collision with M32.

Optical ionised gas offers the perspective especially with the SITELLE instrument to be installed at CFHT (Brousseau et al. 2014). It should enable to map the whole area in several lines with an unprecented sensibility. It will be possible to get the kinematics of the whole area for several optical lines. In order to check the feasibility of this type of work not done since Boulesteix et al. (1987) and get the velocity field, we observed in September-October 2014 with a Fabry-Perot device on T1.6m telescope at Observatoire du Mont-Megantic (Canada) H_α and [NII]. Rubin & Ford (1971) got the only existing data showing that the [NII]/H_α ratio is of order 2-3 in this area. The gas could be dominated by shocks which could explain the absence of star-formation. A similar phenomenon could apply to the CMZ in the Milky Way (Kruijssen et al. 2014).

We thank the IRAM teams for their support for the observations and the data reduction. We thank M. Guélin from making available to us the IRAM-30m M31 large CO survey. We are grateful to Sébastien Viaeney for preparing Herschel data cutouts for us.

References

Azimlu, M., Marciniak, R., & Barmby, P. 2011, AJ, 142, 139
Bacon, R., Emsellem, E., Combes, F., et al. 2001, A&A, 371, 409
Barmby, P., Ashby, M. L. N., Bianchi, L., et al. 2006, ApJ, 650, L45
Bender, R., Kormendy, J., Bower, G., et al. 2005, ApJ, 631, 280
Bergin, E. A., Langer, W. D., & Goldsmith, P. F. 1995, ApJ, 441, 222
Block, D. L., Bournaud, F., Combes, F., et al. 2006, Nature, 443, 832
Boulesteix, J., Georgelin, Y. P., Lecoarer, E., Marcelin, M., & Monnet, G. 1987, A&A, 178, 91
Brousseau, D., Thibault, S., Fortin-Boivin, S., et al. 2014, Proc. SPIE, 9147
Casoli, F., Dupraz, C., Combes, F., & Kazes, I. 1991, A&A, 251, 1
Dame, T. M., Hartmann, D., & Thaddeus, P. 2001, ApJ, 547, 792
Davis, T. A. MNRAS, accepted
del Burgo, C., Mediavilla, E., & Arribas, S. 2000, ApJ, 540, 741
Ford, G. P., Gear, W. K., Smith, M. W. L., et al. 2013, ApJ, 769, 55
Garcia, M. R., Hextall, R., Baganoff, F. K., et al. 2010, ApJ, 710, 755
Kruijssen, J. M. D., Longmore, S. N., Elmegreen, B. G., et al. 2014, MNRAS, 440, 3370
Li, Z., Garcia, M. R., Forman, W. R., et al. 2011, ApJ, 728, L10
Melchior, A.-L., Viallefond, F., Guélin, M., & Neininger, N. 2000, MNRAS, 312, L29
Melchior, A.-L., & Combes, F. 2011, A&A, 536, A52
Melchior, A.-L., & Combes, F. 2013, A&A, 549, A27
Nieten, C., Neininger, N., Guélin, M., et al. 2006, A&A, 453, 459
Rubin, V. C., & Ford, W. K., Jr. 1971, ApJ, 170, 25
Tabatabaei, F. S., & Berkhuijsen, E. M. 2010, A&A, 517, A77
Viaene, S., Fritz, J., Baes, M., et al. 2014, A&A, 567, A71
Wilson, T. L., & Rood, R. 1994, ARA&A, 32, 191